Palaeogeography, Palaeoclimatology, Palaeoecology 692 (2026) 113802

Contents lists available at ScienceDirect

Palaeogeography, Palaeoclimatology, Palaeoecology

journal homepage: www.elsevier.com/locate/palaeo

Unveiling Medusozoan Fossil patterns: A statistical and spatial study of the lower Cambrian Site in Constantina, Spain

Abel Moclán [a,b,*], Alejandro Velázquez-Tello [b], José Ángel Correa-Cano [b], Eduardo Mayoral [c,d]

[a] PALEVOPRIM laboratory, UMR 7262 CNRS and Université de Poitiers, Poitiers, France
[b] Institute of Evolution in Africa (IDEA), Archaeological and Paleontological Museum of Madrid & Rice University, Madrid, Spain
[c] Department of Earth Sciences, University of Huelva, Huelva, Spain
[d] Scientific-Technological Center of Huelva (CCTH), University of Huelva, Huelva, Spain

ARTICLE INFO

Editor: L Angiolini

Keywords:
Medusozoan
Spatial analysis
Taphonomic implications
Corduban
Early Cambrian
Spain

ABSTRACT

A new approach, applying different statistical methods to the early Cambrian medusozoan site of Constantina (Seville, Spain), has allowed the establishment of new biometric parameters for the specimens, a more precise determination of the number of imprints—both subumbrellar and exumbrellar forms—and the deduction of their main taphonomic characteristics. A total of 275 specimens have been identified, with exumbrellar forms (morphotype B) being the most frequent (92%) and having the smallest average length (24.91 cm), while subumbrellar forms (morphotype A) are larger on average (38.29 cm). This new registry represents a record three times greater than previously considered, with the sample characterised by specimens with an average length of 25.93 cm. The analysis of the length/width ratio shows a very strong and statistically significant correlation, implying isometric growth of the medusozoans, consistent with their adult stage. Most specimens exhibit a clear NW-SE orientation, which is parallel to the dominant direction of the palaeocurrents, suggesting that they were reoriented as they were pushed toward the coast before deposition. Additionally, most fossils are clustered in two distinct areas of the surface with very high density, indicating the presence of a common accumulation agent for the entire assemblage. Finally, the analysis of the expanded spatial window through spatial modelling has led to the identification of up to 16 additional specimens that had not been confirmed or were of uncertain identification.

1. Introduction

In the scientific literature, fossils of cnidarian medusae are extremely rare, although references to so-called "medusoid" fossils are relatively common — even if they do not always correspond to genuine body fossils (Young and Hagadorn, 2010). The record of Cambrian medusae fossils is particularly scarce.

The Constantina locality, situated in the Sierra Morena Geopark (Seville, Spain), is one of the few sites preserving hundreds of medusozoan imprints within an early Cambrian (Corduban) intertidal setting (Mayoral et al., 2024; Mayoral et al., 2004). Of comparable age, medusozoan imprints have also been reported from the Zabriskie Quartzite of the southern Nopah Range in the Death Valley region, southeastern California, USA (Sappenfield et al., 2017). A similarly aged site is known from Qingjiang, China (Fu et al., 2019), although the fossils there represent body fossils rather than imprints. In addition, stem-group medusozoans have been documented from the Fortunian Stage of the basal Cambrian (Han et al., 2016).

Nevertheless, most known occurrences correspond to the middle Cambrian (Series 3), such as those from the Burgess Shale, Canada (Devereux, 2001), and from intertidal clastic rocks at several North American localities: the Marjum Formation in the House Range, USA (Cartwright et al., 2007); the Elk Mound Group near Mosinee, USA (Hagadorn et al., 2002; Tarhan and Hagadorn, 2008); and the Potsdam Group at Ausable Chasm, New York, USA, as well as in Quebec, Canada (Hagadorn and Belt, 2008; Lacelle et al., 2008; Tarhan and Hagadorn, 2008).

The revisions carried out by Young and Hagadorn (2010) attribute the specimens from the Elk Mound Group and the Potsdam Group to scyphozoans, while those from the Burgess Shale and the Marjum Formation are assigned, albeit with uncertainty, to hydrozoans or cubozoans. In this context, the oldest crown-group medusae known to date

* Corresponding author at: PALEVOPRIM laboratory, UMR 7262 CNRS and Université de Poitiers, Poitiers, France.
E-mail address: abel.moclan.ramos@univ-poitiers.fr (A. Moclán).

https://doi.org/10.1016/j.palaeo.2026.113802
Received 8 December 2025; Received in revised form 11 April 2026; Accepted 12 April 2026
Available online 13 April 2026

have been found in Utah, within Cambrian Stage 5 (traditional middle Cambrian), whereas no reliable medusae have yet been documented from Series 2, Stage 3 of the Cambrian (Han et al., 2016).

The medusozoan imprints from Constantina occur in medium-grained arkosic greywackes, and the moulds of these fossils reveal radial, ring, and oral canals, as well as short and slender marginal tentacles, displaying a remarkable morphological similarity to extant representatives—a feature already noted by Young and Hagadorn (2010). Furthermore, the absence of disturbance of carcasses by scavengers and/or bioturbating taxa, characteristic of marginal-marine settings of this time (Buatois et al., 2005), and the possible presence of fenestral structures associated with microbial mats, make these fossils comparable to those from the Zabriskie Quartzite (Sappenfield et al., 2017), which represents the oldest recorded medusozoan stranding event, exhibiting very similar taphonomic and sedimentological evidence.

The significance of the Spanish locality lies in the possibility that it represents a precursor assemblage of hydrozoan medusozoans, predating the appearance of the earliest and unequivocal free-swimming macroscopic medusae in the fossil record, such as those found in the Burgess Shale (Raymond Quarry, British Columbia, Canada) (Moon et al., 2023).

Previous work at Constantina (Mayoral et al., 2024; Mayoral et al., 2008; Mayoral et al., 2004) served to characterise the site, and the jellyfish accumulation was interpreted as the result of a mass-mortality event. In this new study, we aim to further investigate the spatial aspects of the accumulation to refine the taphonomic characterisation previously conducted. Thus, the objectives of this work are: i) the application of a series of statistical analyses that allow us to reliably establish the biometric parameters of the imprints, ii) identify possible preferred orientations, iii) determine a precise spatial point pattern to assess the degree of randomness in taphonomic processes, and iv) identify potential additional specimens beyond those that have been definitively confirmed.

2. Constantina site context

This exceptional palaeontological locality is located near the village of Constantina, in the Sierra Morena, about 91 km north of Seville, Spain (Fig. 1). The terminal Neoproterozoic in this area is represented by the marine Volcanic–Sedimentary Complex (Liñán, 1978). Its uppermost part consists of andesites, lutites and fine-grained sandstones belonging to the San Jerónimo Formation, which contains cyanobacteria (Liñán and Palacios, 1983) and trace fossils (Fedonkin, 1985) indicative of a Vendian age. The lower Cambrian succession includes the Torreárboles Formation, the Campoallá Series and the Alanís Beds. The Campoallá Series hosts Ovetian (Atdabanian) archaeocyaths (Perejón, 1984), whereas the Alanís Beds have yielded Marianian (Botoman) trilobites of the *Saukianda* fauna (Richter and Richter, 1940; Sdzuy, 1962).

The fossils described in this study come from the Torreárboles Formation. This unit lies unconformably on the terminal Neoproterozoic basement, which was uplifted in southwestern Iberia during the final Cadomian phases. The resulting pronounced palaeoreliefs were subsequently buried by the Torreárboles siliciclastics, marking the onset of the widespread Cambrian transgression in SW Iberia (Liñán and Gámez Vintaned, 1993). The Torreárboles Formation, which varies between 0 and 400 m in thickness, comprises conglomerates and sandstones of the lower La Tierna Member and reddish shales and sandstones of the upper Julia Member. These deposits reflect an environmental shift from terrestrial and littoral conditions in the lower member to sublittoral settings in the upper one. Trace fossils (Fedonkin, 1985; Liñán, 1984) support a Corduban age for the formation—a north-western peri-Gondwanan stage correlating with the Nemakit-Daldynian and the Tommotian (Liñán and Gámez Vintaned, 1993). The biota examined here comes from the lower part of the La Tierna Member, dated to the earliest Cambrian zone (Gámez Vintaned and Liñán, 1996).

The Constantina site contains one of the densest known concentrations of discoidal soft-bodied fossils from the Phanerozoic. A total of ninety discoid jellyfish specimens were described in previous works as *Cordubia gigantea* Mayoral et al., 2004. These fossils were documented on a single, well-preserved upper bedding surface of approximately 120 m^2 (15 m × 8 m), which dips 20° to the south. Due to the resistant nature of the conglomerates and sandstones of the La Tierna Member, naturally exposed large bedding surfaces are uncommon within the broad outcrops of Spain and Portugal. This circumstance suggests that the previously studied surface was likely revealed artificially in a quarry sometime between the eighteenth and twentieth centuries, when the so-called "house of the written stone"—a structure that inspired the popular interpretation of the fossils as petroglyphs—was constructed nearby using blocks extracted from the La Tierna Member.

The fossils are located on the upper surface of a one-centimetre-thick bed of medium-grained, arkosic greywacke displaying parallel lamination and resting atop a thick conglomerate layer (Mayoral et al., 2024; Mayoral et al., 2008; Mayoral et al., 2004). This greywacke is overprinted by straight-crested, small oscillation ripples that are themselves truncated by the fossils, which appear as gently inclined, shallow furrows broader than they are deep. Several specimens overlap fully or partially (Fig. 2; Fig. 3), and many show an elongation parallel to the palaeocurrent direction. Cross-sections reveal a downward deflection of the horizontal lamination beneath the furrows (see Fig. 2d of Mayoral et al., 2004, p. 194).

Small endogenic burrows (*Planolites montanus* Richter, 1937) and trails (*Cochlichnus* isp.) occasionally overprint both circular and radial

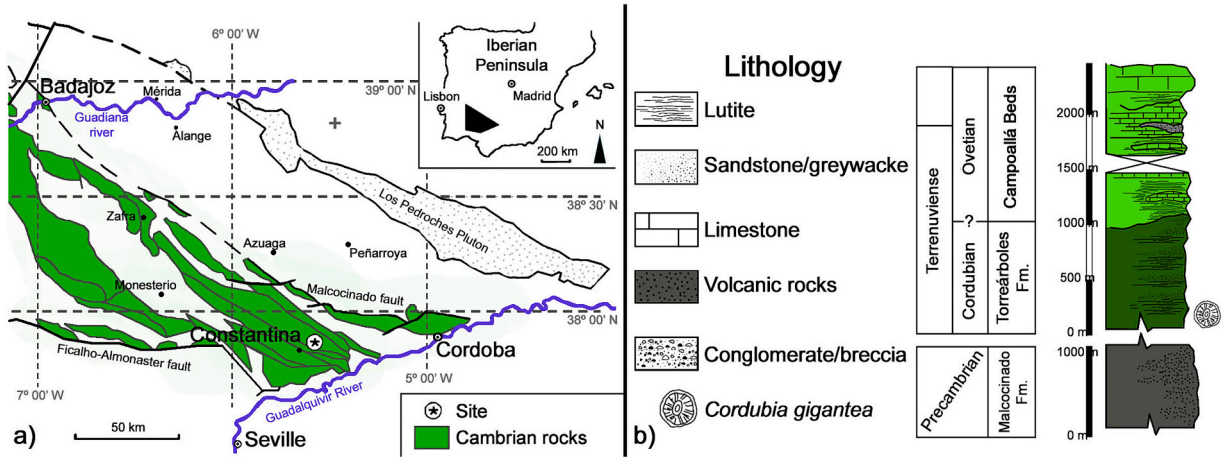

Fig. 1. Left) Location of Constantina site in the Iberian Peninsula and its geological sketch map; right) synthesis of the stratigraphy of the area.

Fig. 2. Detailed pictures of different *Cordubia gigantea* fossils from the Constantina site. a) Subumbrellar imprints, b) Group of totally or partially overlapping subumbrellar and exumbrellar imprints, c) Isolated and overlapping exumbrellar imprints, d) Superimposed exumbrellar imprints. Note the major axis oriented parallel to the palaeocurrent direction of the ripples (white arrow).

Fig. 3. Some general views of *Cordubia gigantea* fossils from the Constantina site. No scale is available for these photographs; to see the sizes of the fossils, see Figs. 2 and 6.

furrows. Additional ichnogenera (including *Monomorphichnus* Crimes and Herdman, 1970 and *Circulichnis* Vyalov, 1971) also occur on the bedding plane. Tectonic joints sharply cut across the furrows, producing slight offsets in a few specimens; this demonstrates that the joints postdate the structures.

The ichnofossil assemblage indicates a marginal-marine community bioturbating a soft, sandy substrate. The small oscillation ripples point to extremely shallow, low-energy conditions. The most plausible interpretation previously proposed (Mayoral et al., 2024; Mayoral et al., 2008; Mayoral et al., 2004) is that a large accumulation of pelagic organisms became stranded along the shoreline during a single episode—likely a mass-mortality event. Rapid burial followed, allowing endobenthic tracemakers to begin bioturbation. This scenario is supported by: (1) overlapping specimens; (2) disruption of ripple marks; (3) deformation of underlying lamination beneath the thickest parts of the bodies while the sediment remained unconsolidated; (4) elongation of certain fossils parallel to palaeocurrents, consistent with deformation at the time of deposition; (5) their unexpectedly good preservation in coarse siliciclastic sediment; and (6) overprinting by trace fossils.

3. Material and methods

3.1. Spatial documentation

During the conservation phase of the site and the preparation of the necessary proposed subsequent musealisation (Mayoral et al., 2021; Mayoral et al., 2019), two photogrammetric models were created to document the analysed surface both during and after the intervention, as

well as to facilitate the identification of the fossils after fieldwork. The photogrammetry was conducted at different times of the day to generate orthophotos (Fig. 4) with distinct lighting conditions (vertical and grazing lighting), enhancing the visibility of the fossils. The photogrammetric models were produced using Agisoft Metashape software ver. 1.8.

Additionally, using a Nikon total station (DTM-322), we mapped several reference points at the site, allowing us to georeference the orthophotos within a local coordinate system. The north of the coordinate system was aligned with magnetic north using a compass on May 11, 2024.

The cartographic documentation of the fossils was carried out by creating polygonal layers using ArcGIS 10.8. The identification of the fossils was conducted through a detailed analysis of the georeferenced orthophotos in ArcGIS and by analysing the photogrammetric model with varying light conditions using Blender 4.2. This approach was chosen because, during fieldwork, we observed that many of the fossils were not visible depending on the lighting conditions, making office-based documentation more efficient. However, it is true that during the fieldwork, we documented as many fossils as possible to compare them with the subsequent analysis. In any case, this step carried out in Blender was particularly important, since the imprints were at a slightly lower elevation than the analysed surface. This meant that the incidence of grazing light allowed for better visualisation of the imprints in most cases. In any event, the review of the accepted cases was conducted separately by each of the authors in order to confirm the secure attributions and those that were more doubtful.

Additionally, we also documented the position of the main joints affecting the analysed surface and especially those that were so large that they erased significant areas of the surface, which we were therefore unable to analyse.

Once we had the polygon layer completed, we generated a point layer from the polygons to obtain the *xy* coordinates of the centroids of each fossil through the *Feature to Point* function (selected features: Inside (optional)*: checked*). From there, also using ArcGIS, we calculated the area and perimeter of the traces and, through the Minimum Bounding Geometry function (selected features: Geometry type*: rectangle_by_width;* Group option*: none;* Add geometry characteristics as attributes to

Fig. 4. Orthophotographic models developed to document and to analyse the Constantina palaeontological surface.

output*: checked*), we obtained a new polygon layer, with which we were able to calculate the length (major symmetry axis), width (minor symmetry axis), and orientation (from 0 to 180°) of each specimen. In this way, all measurements and coordinate calculations were performed automatically and objectively by the software. Next, we exported the provided dataset in table format to conduct statistical analysis with it (Supplementary File 1).

During the GIS-based documentation of the fossils, we differentiated between jellyfish that typologically corresponded to subumbrellas (morphotype A) and those corresponding to exumbrellas (morphotype B). This distinction was made following the visual criteria shown in Fig. 5 and previously proposed in other studies (Mayoral et al., 2024; Mayoral et al., 2008; Mayoral et al., 2004). The subumbrellas are the most complex in morphological terms, corresponding to the ventral part of the jellyfish, and are characterised by the presence of the imprint of the mouth, the mouth canal, the radial canals, and the ring canal. In turn, the exumbrellas, which are identified with the dorsal part of the jellyfish, are characterised solely by the presence of the ring canal, with no other imprint occurring within the area occupied by the fossil.

3.2. Statistical analysis

First, we analysed the metric variability of the sample, examining both the length and width, as well as the perimeter and area of the fossils. For this, we used a basic approach to descriptive statistics, i.e., mean, median, standard deviation, and 95% confidence interval of the mean, and created violin/boxplots for these variables. Next, we analysed the normality of the sample based on the morphotype of the fossils (i.e., Morphotype A, Morphotype B) and then compared both morphotypes at the metric level using a Wilcoxon test. We then specifically focused on the metric relationships between the length and width of the traces, performing a Spearman correlation with the entire sample and differentiating by morphotypes. Finally, we also conducted a linear regression with the sample. These analyses were performed using R software (R Core Team, 2022, with the 'ggplot2' library (Wickham, 2016) to create the graphical material. All analyses and the code used can be found in Supplementary File 2.

We analysed the orientation of the fossils based on the information obtained with the Minimum Bounding Geometry. We conducted this analysis with the aim of identifying possible preferential orientations in the analysed sample that could help us identify potential water currents that may have oriented the sample. This is useful in different contexts, whether of low or high energy (Cobo-Sánchez et al., 2014; Domínguez-Rodrigo et al., 2014; Domínguez-Rodrigo and García-Pérez, 2013; Méndez-Quintas et al., 2019). The data were analysed using the PAST 4.03 software (Hammer et al., 2001) through the 'CIRCULAR, ONE SAMPLE' function (selected features: *rose plot; Axial (orientation); equal area; mean; counts*). Being aware that the circularity of the traces could pose a challenge for this analysis, we calculated an elongation index (length/width) before performing the analysis. This allowed us to obtain values >1. We excluded all values <1.1 and performed an initial analysis with all the remaining samples. However, since this could still be insufficient, we also conducted the analysis with the fossils having elongation indices ≥1.5. To interpret the possible preferential orientation, we used the tests included in PAST 4.03 for this purpose (Rayleigh's R, Rao's U, and χ^2).

On the other hand, we conducted an analysis of the spatial point pattern (Baddeley et al., 2016; Wiegand and Moloney, 2013) of fossils. Spatial analyses are of great interest in taphonomic studies (Domínguez-Rodrigo et al., 2018) because they allow us to assess, among other aspects, the degree of randomness in taphogenic processes (e.g. Arteaga-Brieba et al., 2023; Cobo-Sánchez et al., 2024; Diez-Martín et al., 2021; Luzón et al., 2021; Martín-Perea et al., 2020; Mielgo et al., 2024; Sánchez-Romero et al., 2020). This aspect is especially crucial when we want to analyse whether fossil accumulations have a synchronous or penecontemporary origin, or to assess the degree of alteration by taphonomic agents, such as water (Domínguez-Rodrigo et al., 2018).

The application of these methods to contexts with fossils has been extensively explored, particularly in Ediacaran sites. In these studies, one of the most significant aspects is analysing the degree of randomness in point patterns to interpret factors such as the distribution of food resources or the reproductive strategies of organisms (Boan et al., 2024; Boan et al., 2023; Coutts et al., 2018; Dhungana and Mitchell, 2021; Kolesnikov, 2022; Mitchell et al., 2015; Mitchell and Butterfield, 2018; Mitchell and Kenchington, 2018; Pohle et al., 2020; Rojas et al., 2020).

Since we have observed that all the metric variability of morphotype A is contained within the metric variability of morphotype B (see Results), we conducted the spatial analysis using the complete sample, avoiding subdividing the dataset according to morphotypes.

The analysis began with a study of the spatial intensity (number of

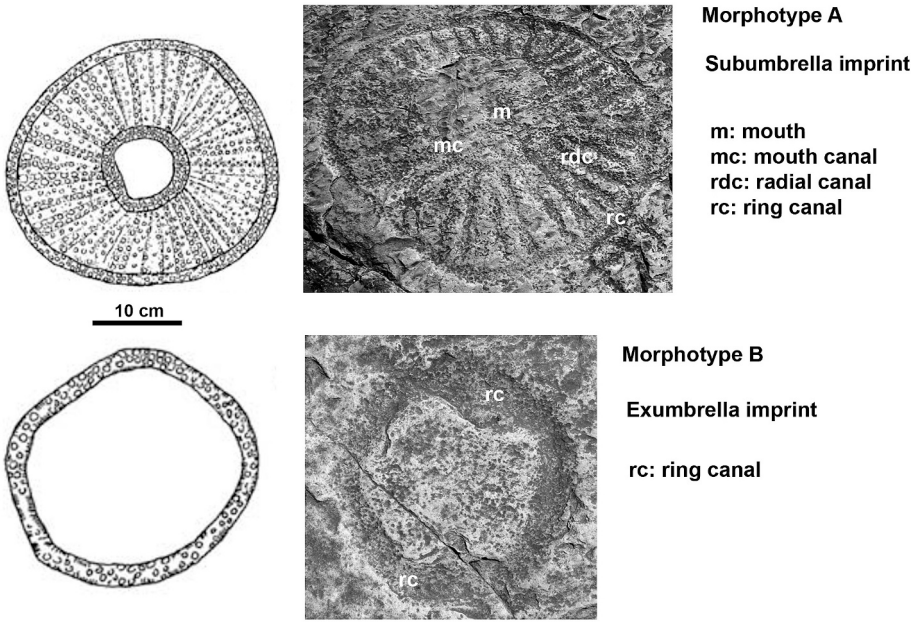

Fig. 5. Typology of jellyfish identified in Constantina and their diagnostic features.

points per unit area) of the sample by creating a kernel intensity map and analysing which areas had significant intensity at the 99% confidence level (hotspot analysis). It must be noted that these maps cannot be used on their own to characterise the degree of randomness in a spatial point pattern. Intensity maps show where points are concentrated, whereas hotspot maps indicate where those points are statistically more significant. However, the presence of high-intensity areas in either intensity or hotspot maps does not necessarily imply the existence of clustering or regular distributions; these must be identified through the use of specific statistical tests (Baddeley et al., 2016). We state this because, in an intensity map, there will always be areas with a higher intensity of points than others, which are then displayed as the most intense zones. The presence of these high-intensity areas can occur in random (i.e., absence of spatial relationship between points), regular (i.e., negative association between points/segregation), or clustered (i.e., positive association between points/aggregation) spatial distributions; therefore, these two types of maps cannot be used to reject the null hypothesis of Complete Spatial Randomness (CSR).

Then, we identified the typology of the point pattern to provide a better taphonomic characterisation of the site. To do this, we employed different methods to test the null hypothesis of randomness in the sample after verifying, using a χ^2 test (with four different grids: 5 × 5, 8 × 8, 10 × 10, 12 × 12), that the sample is inhomogeneous (χ^2 test p-value <0.05; see Results section). This step is crucial because the subsequent tests depend directly on whether the point pattern is homogeneous or inhomogeneous. For instance, if we wish to use a K-function to analyse the randomness of the point pattern, we must apply the standard K-function for a homogeneous distribution or the inhomogeneous K-function if the distribution is inhomogeneous. This is comparable to univariate or bivariate statistics, where, before analysing the mean of a measurement, we first determine whether the distribution is normal or non-normal to then choose between parametric or non-parametric tests.

The selected tests included the Hopkins-Skellam test, the Clark-Evans test, the DCLF (Diggle-Cressie-Loosmore-Ford) test, and the MAD (Maximum Absolute Deviation) test, using the inhomogeneous K, L, F, G, and J functions, as well as the scaled K and L functions. Similarly, we used the K, L, F, G, and J inhomogeneous functions and the scaled K and L functions to graphically describe the behaviour of the spatial point pattern. All of these functions aim to characterise the nature of the spatial point pattern (i.e., CSR, regular or clustered) while taking its intensity (K, L functions) or neighbourhood (Hopkins-Skellam and Clark-Evans tests, F, G and J functions) into account, starting from the null hypothesis of spatial randomness and considering as alternative hypotheses the presence of clustering or of regular distributions. Thus, in most cases, it is advantageous to employ all these tests simultaneously, as a spatial distribution may be more sensitive to analysis based on either neighbourhood or intensity. Consequently, it is possible for the K and L functions to yield positive results while the F, G, and J functions do not, or vice versa.

Finally, we used the 'nnclean' function to detect possible clustering (the test assumes clustering when performed, which is why the existence of clustering must be confirmed beforehand using the functions) of materials through nearest neighbour clutter removal. This method is particularly useful because it analyses the point pattern based on neighbourhood (or proximity) between points rather than on the intensity of the spatial point pattern, as previously done by the intensity and hotspot maps. Furthermore, this approach allows for the assessment of the probability with which the test considers points to be part of a cluster, which aids in better understanding the cluster radius and the interdependence between points.

To further investigate the spatial point pattern, we fit four different Poisson point process models (linear, quadratic, cubic, and 4th degree polynomial). The modelling process allows us to estimate the potential fossil intensity in areas of the site that remain unexcavated or have been lost to erosion. Furthermore, it serves as a highly valuable support system for understanding the site's intensity; if the modelled intensity does not align with the observed intensity, we can detect areas of special interest that deviate from the general trend of the spatial model. The models were evaluated using the Akaike Information Criterion (AIC) index, and subsequently, we compared their validity through ANOVA. Finally, we selected the best-performing model (i.e., the one with the lowest AIC values) and generated four maps: 1) estimated intensity of the point process based on the fitted model, 2) simulation of a new point pattern using the fitted model with the Metropolis-Hastings algorithm, 3) a difference map subtracting the intensity of the simulated new point pattern from the "real" intensity of the spatial point pattern and 4) an extrapolated estimation of potential points within a larger spatial window (525 m^2) than the original one. We could say that these methods are, to some extent, the spatial equivalent of a regression, which is why they are especially useful here for assessing, using different methods, how the intensity of the point pattern is and how much of the site might not have been studied due to erosion or because it is still covered. Both the code and the results of these analyses are presented in Supplementary File 3.

In summary, the methods employed follow a logical sequence that addresses all the requirements of a spatial analysis: 1) Exploratory intensity maps; 2) testing for homogeneity/inhomogeneity; 3) characterisation of the point pattern typology (i.e., CSR, clustering, or regular distribution); and 4) spatial modelling to define the general pattern and estimate point density in unknown areas.

All these analyses were performed using R software (R Core Team, 2022) and the 'spatstat' library (Baddeley et al., 2016; Baddeley and Turner, 2005). The data used for the analysis were the *xy* coordinates of the fossil centroids. For an extensive explanation of the use and application of these methods, see previous works (Moclán et al., 2023b; Moclán et al., 2023a).

All maps were created using a spatial window that we defined based on the orthophotographs, covering an area of 125.48 m^2 with a major axis of ~19.84 m. It is worth noting that during the spatial analysis, we excluded the areas occupied by the main joints of the site, which therefore prevented the evaluation of the presence of fossils in those areas. All coordinates related to the spatial window are included in the Supplementary File 4.

4. Results

The documentation work conducted has served to document a total of 275 specimens of *Cordubia gigantea* at the Constantina palaeontological site (Fig. 6). This implies that the known sample has been tripled to date (Mayoral et al., 2021; Mayoral et al., 2008; Mayoral et al., 2004). Likewise, we have identified 14 traces that, although they could represent new specimens, we are unsure of their identification, so we have chosen to exclude their presence in the subsequent analyses (Fig. 6a). Regarding the typology of the fossils, a total of 21 have been identified as subumbrellas (morphotype A), while a total of 254 have been characterised as exumbrellas (morphotype B).

At the metric level, we observed significant variability in the analysed sample, with fossils ranging from 7.74 cm to 102.47 cm in length (Table 1). However, we found that the larger and especially small specimens are generally uncommon (Fig. 7), with the average length of the sample being 25.93 cm, and the confidence interval ranging from 24.23 to 27.64 cm. If the fossils are analysed based on morphotype, we can see that, regardless of the variable analysed, fossils of morphotype A tend to be larger on average (Length mean = 38.29; Length median = 34.58) than those of morphotype B (Length mean = 24.91; Length median = 22.24), which show a distribution very similar to the mean value of the entire population.

When performing a Shapiro-Wilk test on the variables length, width, perimeter, and area for both morphotypes, we observed that all samples exhibited a non-normal distribution (p-value <0.05; see Supplementary File 2). This led us to use a Wilcoxon test to compare the mean metric values of the samples, and it was found that there are statistically

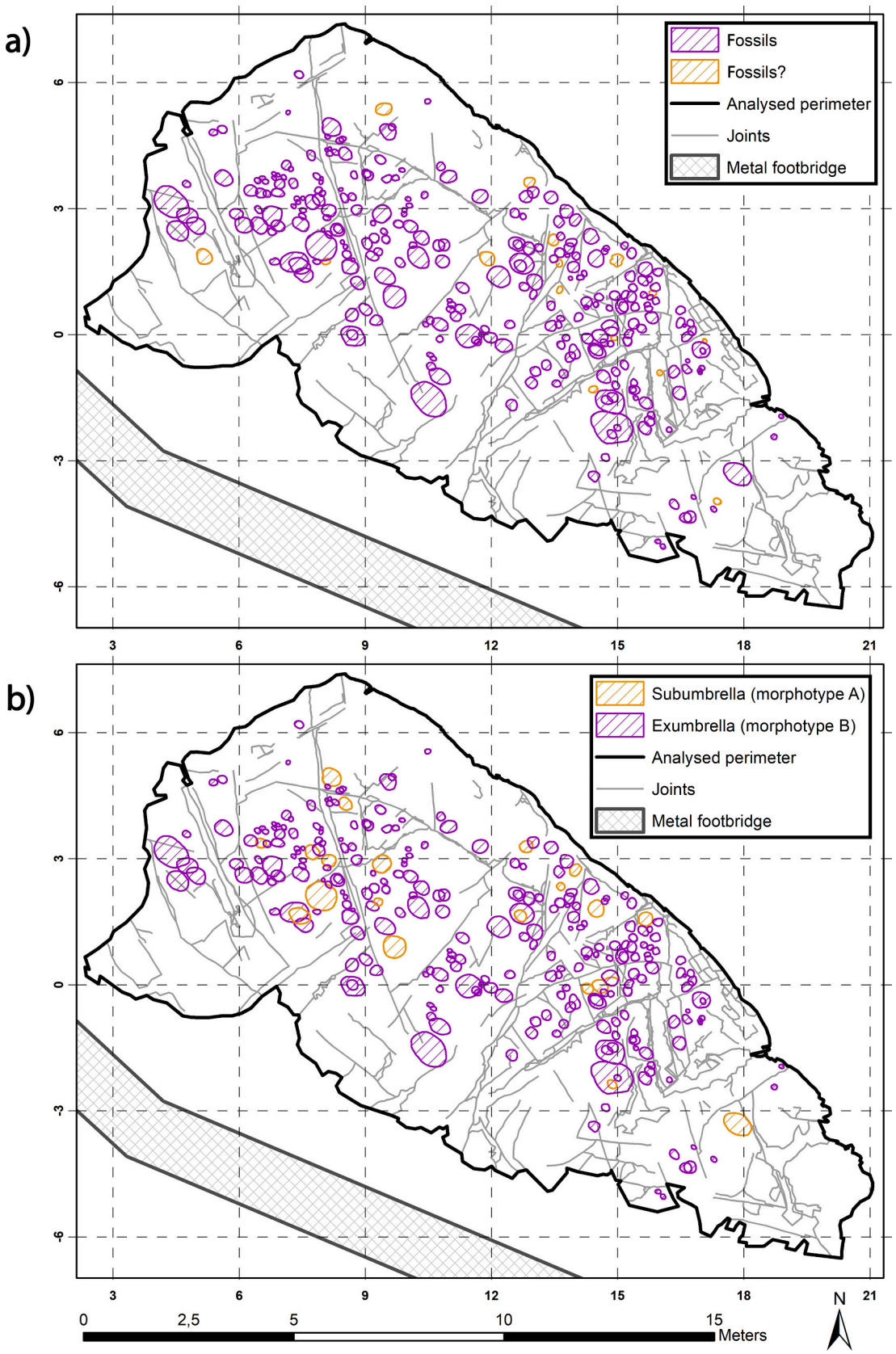

Fig. 6. a) Spatial distribution of the identified fossils and location of those unclear traces. b) Spatial distribution of *Cordubia gigantea* fossils depending on the morphotype.

Table 1
Descriptive statistics of the analysis sample.

	A + B (n = 275)	A (n = 21)	B (n = 254)
Length			
Minimum	7.742	19.471	7.742
Maximum	102.47	75.371	102.47
Mean	25.933	38.285	24.912
Median	22.811	34.579	22.239
Standard deviation	14.337	14.800	13.841
CI 95% (lower)	24.231	31.548	23.201
CI 95% (upper)	27.635	45.023	26.622
Width			
Minimum	6.919	17.353	6.919
Maximum	74.675	65.436	74.675
Mean	20.764	31.725	19.857
Median	18.396	28.818	17.834
Standard deviation	10.944	12.382	10.334
CI 95% (lower)	19.464	26.088	18.580
CI 95% (upper)	22.063	37.361	21.134
Perimeter			
Minimum	0.235	0.028	0.235
Maximum	2.838	0.393	2.838
Mean	0.744	1.112	0.713
Median	0.654	1.007	0.639
Standard deviation	0.401	0.426	0.384
CI 95% (lower)	0.696	0.918	0.666
CI 95% (upper)	0.791	1.306	0.761
Area			
Minimum	0.004	0.605	0.004
Maximum	0.588	2.242	0.588
Mean	0.054	0.109	0.050
Median	0.032	0.078	0.031
Standard deviation	0.072	0.090	0.069
CI 95% (lower)	0.046	0.068	0.041
CI 95% (upper)	0.063	0.150	0.058

significant differences between the morphotypes in all four variables (p-value <0.05; see Supplementary File 2).

If we analyse the relationship between the length and width of the fossils (now excluding area and perimeter, as they are closely related to the former) through a Spearman's correlation (this method is chosen due to the non-normality of the samples), we observe a very strong and statistically significant correlation, regardless of whether we analyse the measurements of the complete sample (r = 0.97; p-value = 1.17×10^{-169}), morphotype A (r = 0.974; p-value = 4.85×10^{-6}), or morphotype B (r = 0.967; p-value = 3.28×10^{-152}). This strong correlation is also observed when we perform a linear regression between length and width (Table 2; Fig. 8), yielding R^2 values higher than 0.9 and highly significant p-values (<0.05).

The analysis of the orientation of the sample has revealed a clear northwest-southeast trend, regardless of whether the sample is analysed with an elongation index of ≥1.1 or ≥ 1.5 (see Fig. 2d). Statistically, this observation, made with rose diagrams (Fig. 9), is reinforced by the various tests used to measure the presence of preferential orientations. In the sample with an elongation index of ≥1.1 (circular mean = 117.84; 95% CI = 113.4–122.3), Rayleigh's test (R = 0.53; p-value = 9.43×10^{-29}), Rao's U test (U = 171.3; p-value = 0), and the χ^2 test (χ^2 = 141.5; df = 7; p-value = 2.48×10^{-27}), show the existence of preferential orientations. This is also the case for samples with an elongation index of ≥1.5 (circular mean = 114.26; 95% CI = 96.63–131.9), although the Rayleigh's (R = 0.54; p-value = 0.008), Rao's (U = 165.5; p-value = 0.047) and χ^2 (χ^2 = 9; df = 3; p-value = 0.029) tests show slightly higher p-values due to the smaller sample size.

The spatial analysis performed on the centroids (Fig. 10) revealed a spatial intensity of 2.27. When visualising the kernel intensity map (Fig. 11), we observe that most of the studied area has very low intensity, with most of the fossils "clustered" in two distinct areas of very high intensity. In addition, these areas correspond to surfaces where the

Table 2
Results obtained by the linear regression analysis.

Morphotype	Intercept	Slope	p-value	R^2
A + B	1.493	0.743	6.20E-177	0.948
A	1.181	0.798	2.34E-11	0.909
B	1.726	0.728	2.74E-166	0.95

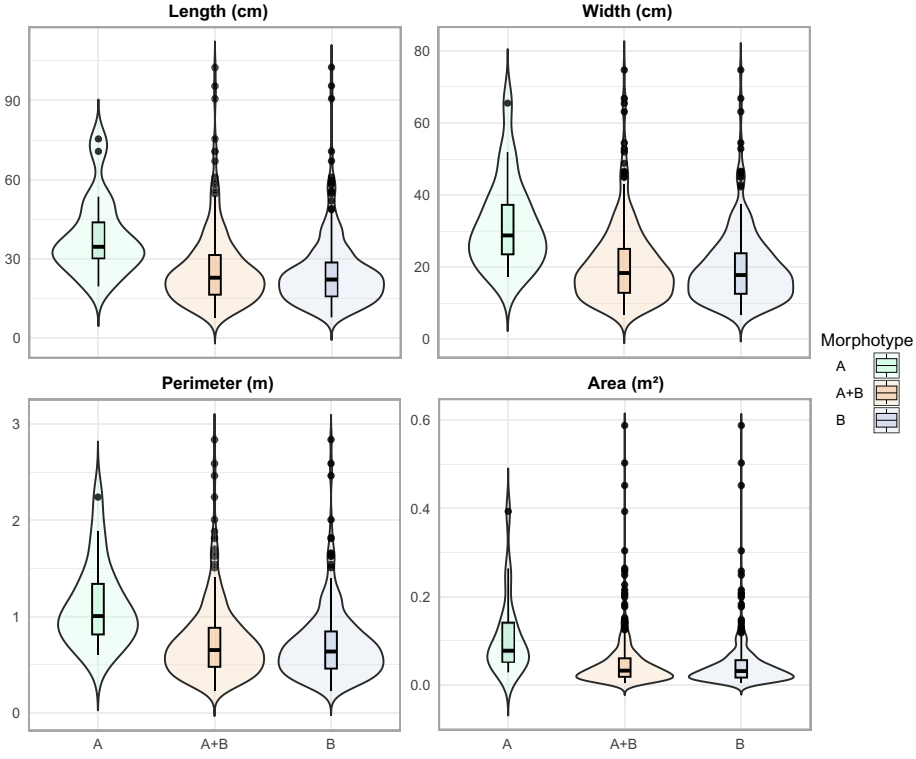

Fig. 7. Violin plots comparing the metric values of length, width, area, and perimeter for the two morphotypes and the complete sample.

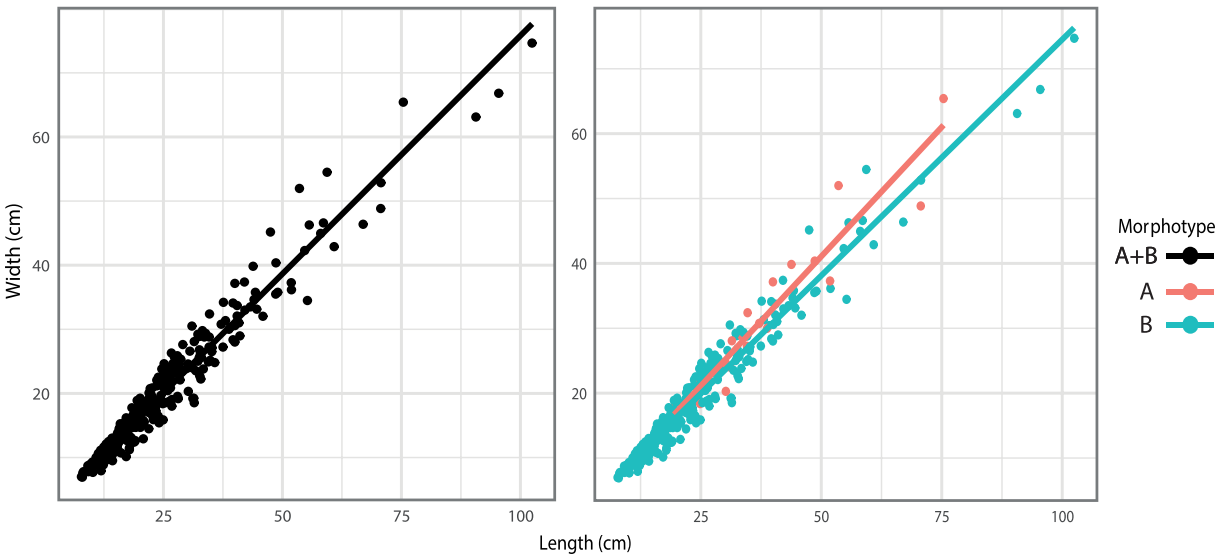

Fig. 8. Linear regression performed with the entire sample (left) and by morphotypes (right).

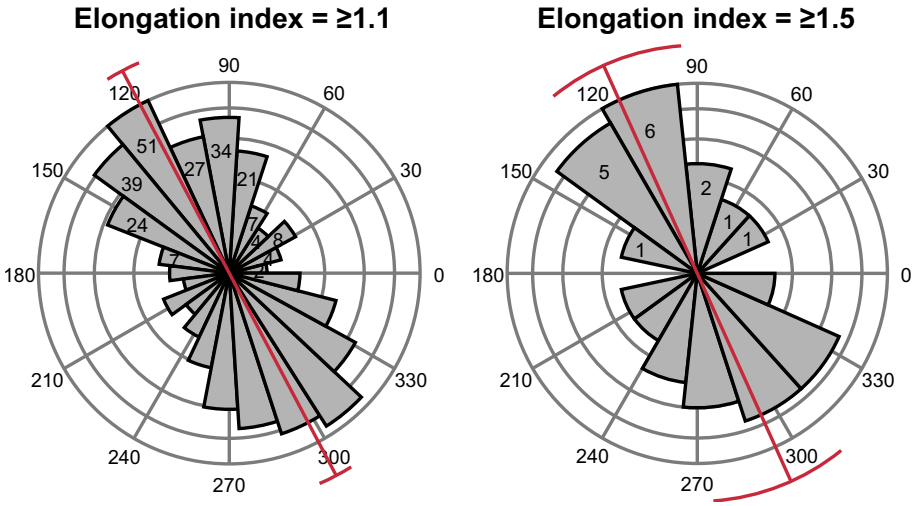

Fig. 9. Rose diagram created with specimens that have an elongation index of ≥1.1 (left) and ≥ 1.5 (right). (For interpretation of the references to colour in this figure legend, the reader is referred to the web version of this article.)

intensity is highly significant, exceeding the 99% CI (Fig. 11c, d).

Next, we analysed the homogeneity of the spatial pattern using 5 × 5 ($\chi^2 = 293.84$; df = 18; *p*-value = 1.78×10^{-51}), 8 × 8 ($\chi^2 = 291.656$; df = 42; p-value = 8.37×10^{-39}), 10 × 10 ($\chi^2 = 337.66$; df = 67; p-value = 1.93×10^{-37}), and 12 × 12 ($\chi^2 = 407.38$; df = 93; p-value = 1.26×10^{-40}) grids through a χ^2 test. The results clearly indicate that the sample is inhomogeneous, requiring the use of appropriate functions for such point patterns. We also attempted to identify the type of inhomogeneity present in the sample, but the sample size was too small to perform a studentised permutation test (see warnings and errors in Supplementary File 3: code lines 98–114). Therefore, we decided to analyse the spatial point pattern using both classical inhomogeneous functions and scaled functions.

First, we applied the Clark-Evans and Hopkins-Skellam tests, which suggest the presence of a clustered spatial pattern. However, these tests are highly sensitive to inhomogeneity and may misinterpret it as clustering when the pattern is clearly inhomogeneous (Baddeley et al., 2016). Given the inhomogeneity of our sample, these results should be interpreted with caution.

Next, we employed the DCLF and MAD tests using the K, L, F, G, and J functions, as well as the Kscaled and Lscaled functions. The obtained *p*-values were < 0.05 for the K, L, Kscaled, and Lscaled functions, meaning that the null hypothesis of randomness could not be rejected for the remaining functions (p-value >0.05). When applying the functions, the results were consistent with these findings (Fig. 12). Specifically, the F, G, J, and Pair Correlation functions did not reject the null hypothesis of randomness, while the Kscaled and Lscaled functions indicated the presence of a clustered pattern at distances of 0.5–1 m. In contrast, the K and L functions suggested a clustered pattern at short distances (0.5–1 m) and a regular pattern beyond 2–2.5 m.

The application of the nearest neighbour clutter removal (Fig. 13) also supports that, regardless of whether we analyse the sample with *k*-values of 5, 10, or 20, certain areas with fossils likely exhibit a clustered pattern. These areas correspond to the two focal points observed in the intensity and hotspot maps (Fig. 11c-d).

Finally, the fitting of Poisson process models generated models that, according to the ANOVA analysis, are useful for describing the intensity of the spatial point pattern (low AIC values and significant p-values). However, the best-fitting model is the most complex one, i.e., 4th degree polynomial, as evidenced by having the lowest AIC value (−199.291) of all and by significantly improving the cubic regression according to ANOVA (see Supplementary File 3). The predicted intensity map

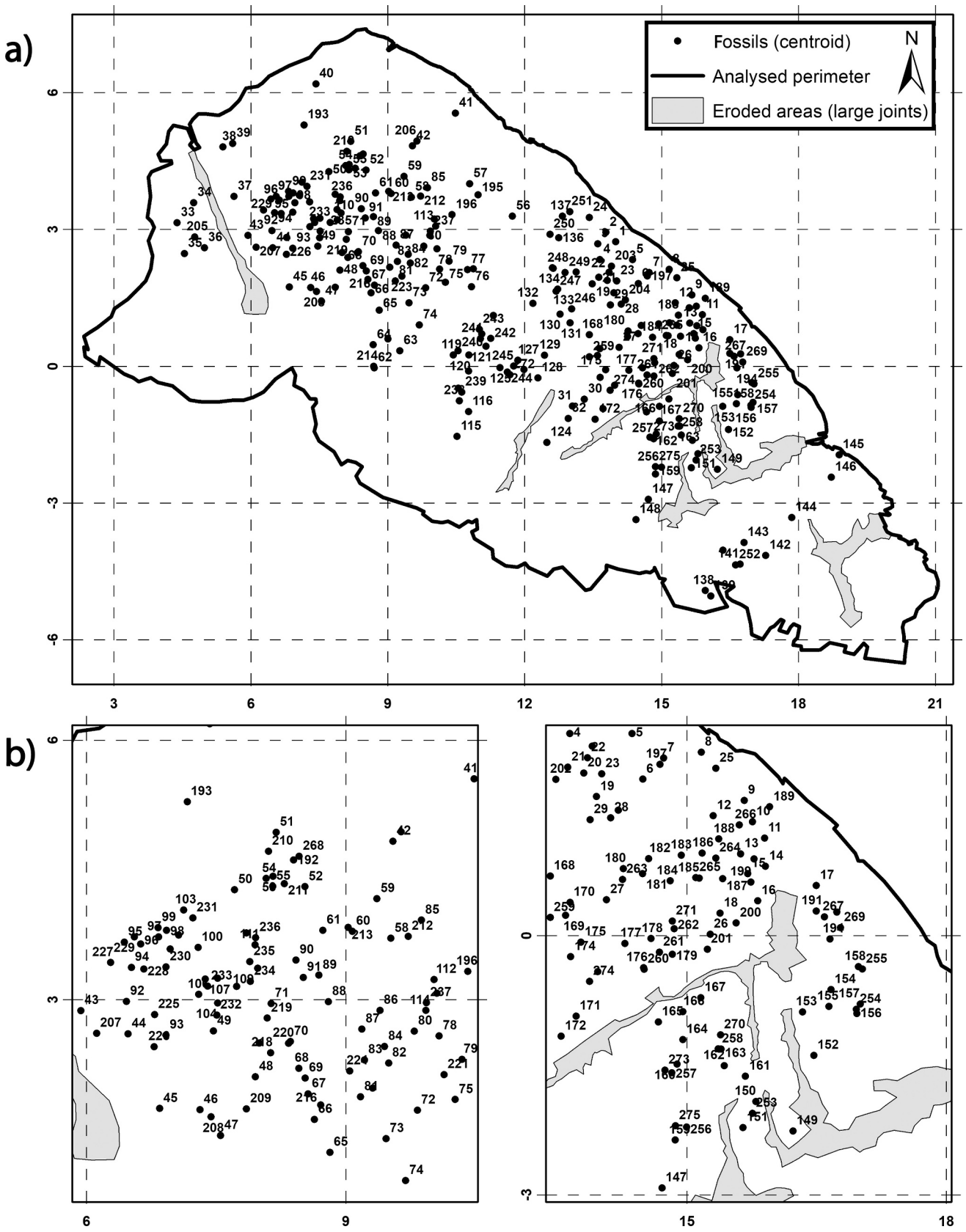

Fig. 10. a) Spatial distribution of the centroid of each fossil; b) and c) detailed areas with high concentrations of fossils.

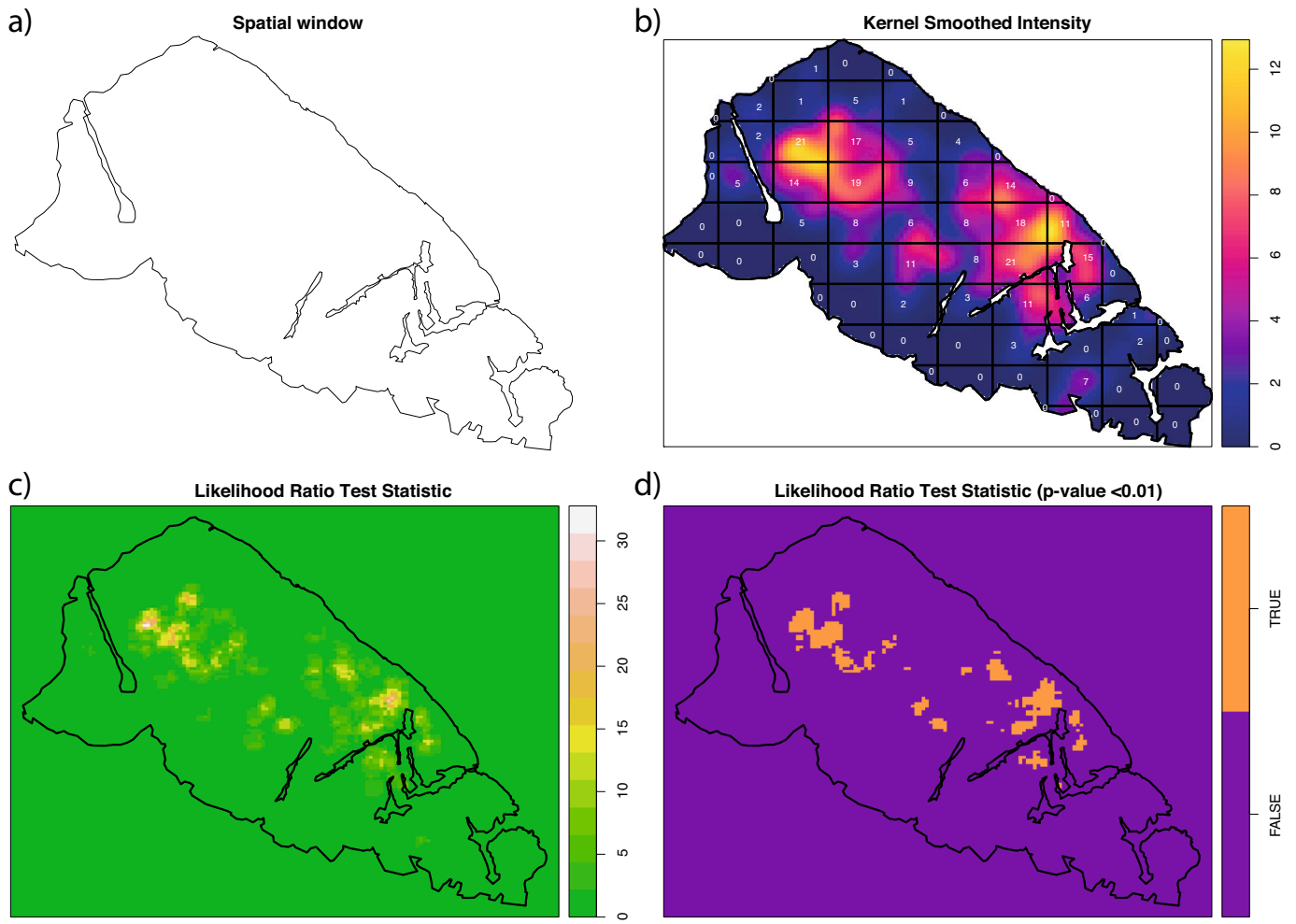

Fig. 11. a) Detail of the spatial window and the joints that were excluded from the analysis; b) Kernel smoothed intensity map; c) Hotspot; d) Areas where intensity is significant above the 99% CI.

(Fig. 14a) and the intensity map of the simulated new point pattern show two distinct areas of high intensity, similar to the original point pattern intensity map (Fig. 11b). As seen in the presence of red zones in Fig. 14c, these high-intensity areas appear to be highly significant, with real intensity values much higher than expected by the models.

The analysis of a larger spatial window (Fig. 14d) estimated the presence of 291.60 specimens, implying only about 16 more fossils than those already identified. This is particularly relevant, as some specimens have been observed outside the original window and within the space of some of the joints.

5. Discussion

Previous studies conducted at the site (Mayoral et al., 2021; Mayoral et al., 2019; Mayoral et al., 2008; Mayoral et al., 2004) suggested that the faunal accumulation must have formed rapidly, based on several criteria, including the superposition of specimens and the elongation of some specimens parallel to the direction of the ripple current. The presence of a clustered spatial pattern, which appears to be confirmed by the K and L functions—regardless of whether inhomogeneous or scaled versions are used—as well as by the DCLF and MAD tests with these same functions, provides additional support for the idea that there is indeed an aggregative association among the specimens. The fitting of spatial models confirms that this spatial point pattern is accurate, making it particularly interesting to observe that the identified clusters indeed exhibit a much higher intensity than expected. Thus, this spatial point pattern can only be explained taphonomically by the presence of a common accumulating agent for the complete assemblage.

Theoretically, there are other possible alternatives that could explain the bimodal cluster pattern of the specimens. Thus, in sedimentology, topographic depressions act as sediment traps where particles and organic remains accumulate due to locally reduced flow velocities and subsequent burial, a principle widely acknowledged in depositional models (e.g. sediment traps; Ritter, 1972). Accordingly, for a surface to function as a trap for the accumulation of jellyfish bodies, physical depressions with depths comparable to the vertical size of the organisms would be required, as these would be most effective in slowing currents and promoting deposition prior to burial. This is a logical interpretation based on physical and sedimentological principles. In our case, *Cordubia* was a discoidal jellyfish with a mean diameter of approximately 25 cm. Its bell was likely "flattened" or shallow-domed, meaning its vertical height would have been significantly smaller than its diameter—likely one-third or slightly more, implying a height of at least 8–12 cm. This mechanism would require depressions of comparable depth across the bedding surface, which are not observed at any point.

Furthermore, transitions from medium to finer grain sizes (finer sand or silt) within a sandy surface could act as zones where flow energy dissipates and bodies settle. This feature is also absent across the surface, which is composed entirely of medium-grained arkosic greywackes. Additionally, transport thresholds for particle deposition imply that large bodies cease movement only when local flow energy falls below critical values (van den Berg and Nio, 2010). In our case, the concentrations of fossil bodies were likely controlled jointly by surface geometry and flow dynamics through transport and deposition processes

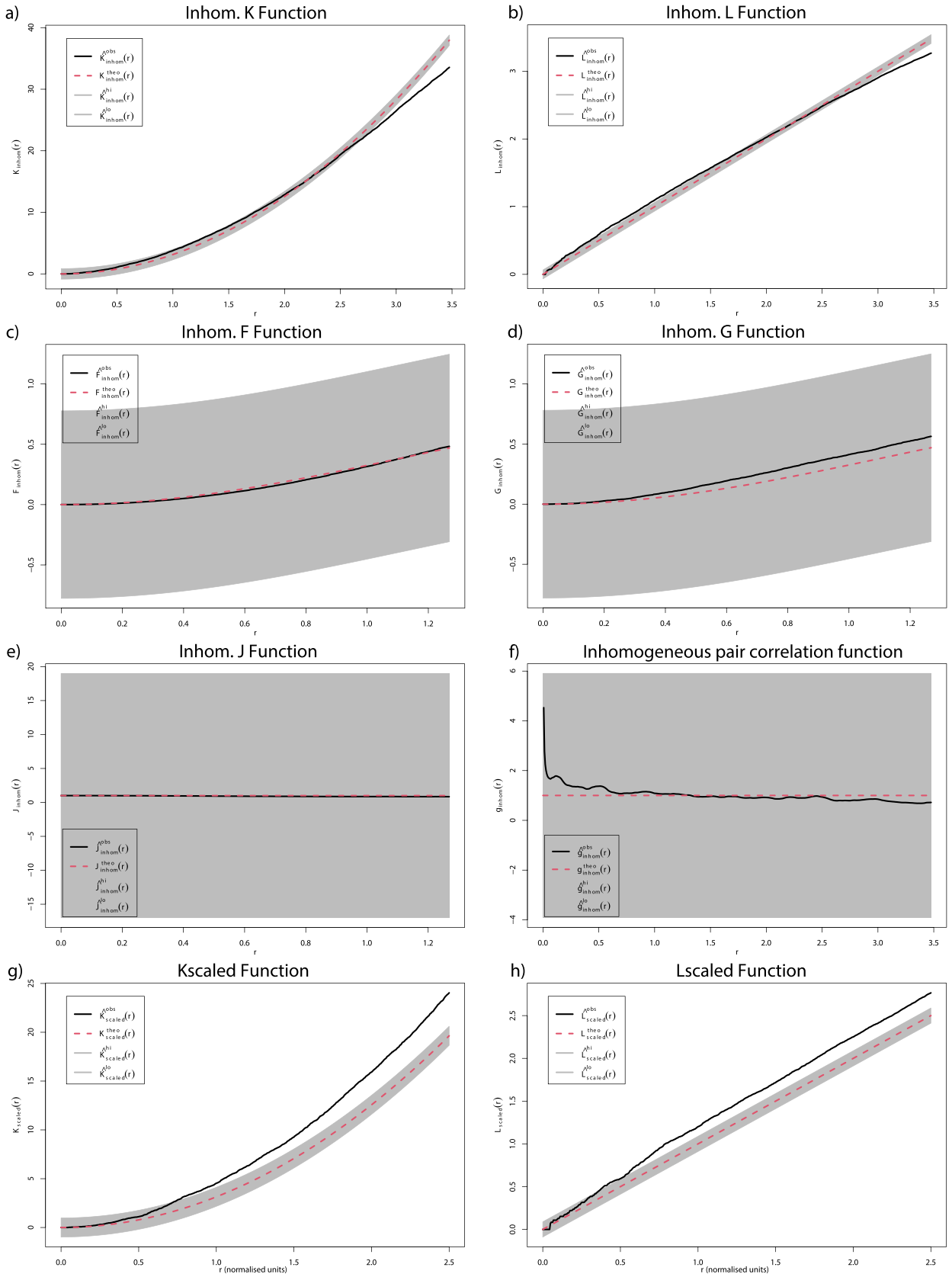

Fig. 12. Different inhomogeneous functions used in this study.

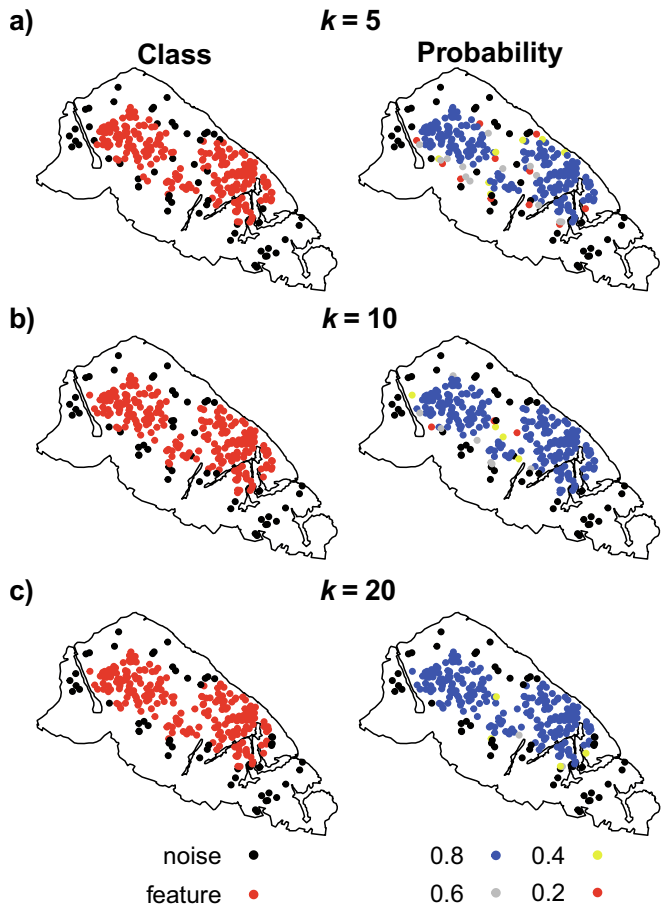

Fig. 13. Results provided by the nearest neighbour clutter removal analysis.

(condensation and trap effects), conditions widely recognised in taphonomic models (Fernández-López et al., 2002).

What we know so far about water currents suggests that the specimens should not accumulate in a clustered pattern. Instead, water, as a taphonomic agent, would likely tend to disperse remains and generate spatial point patterns of a random nature (Domínguez-Rodrigo et al., 2018). However, these assumptions have been based on vertebrate organisms in fluvio-lacustrine contexts, so in the case of jellyfish in marine environments, this pattern may not necessarily be the same. Thus, we consider that the identification of a clustered pattern in a case like this—on a beach with very low energy—likely does not correspond in any way to fluvial hydrodynamic models.

Therefore, the spatial analysis confirms the hypothesis that the specimens likely died during a mass mortality event triggered by an ecological stress event and were subsequently transported to the beach. Likewise, the existence of a preferred orientation in the accumulation of specimens further supports this idea, as they were reoriented in alignment with the low-energy current, as proposed by Mayoral et al. (2004).

Morphotype B (exumbrellar side) is smaller than Morphotype A (subumbrellar side). This smaller size may have made it easier for them to be transported by currents, increasing their chances of reaching the beach (Fossette et al., 2015; Gemmell et al., 2013). Once on the beach, these smaller specimens, if deposited in a subumbrellar position, could have been more easily flipped over by the current, ending up in an exumbrellar position (Sappenfield et al., 2017). Once stranded on the beach, jellyfish lose almost all capacity for active movement due to rapid collapse and dehydration of the gelatinous bell, which is composed of more than 95% water. As a result, they are unable to actively reorient themselves after deposition. However, their orientation may still change passively due to physical processes acting on the shoreface. Wave oscillations, swash and backwash currents, or wind-driven movements can overturn stranded individuals, especially smaller or lighter ones, leading to random alternation between subumbrellar and exumbrellar positions. This explains why stranded jellyfish of species such as *Aurelia aurita* Linnaeus, 1758 or *Velella velella* (Linnaeus, 1758) are commonly observed in both orientations on beaches today. Therefore, post-depositional overturning of stranded medusae should be interpreted as a physically induced, not biologically controlled, process (Betti et al., 2019; Fossette et al., 2015; Gemmell et al., 2013; Jones et al., 2021).

In general, most modern jellyfish strand on the beach with their oral side facing downward (subumbrella down). However, some jellyfish, like those of the *Cassiopeia* genus, swim "upside down" (oral side facing up) and may also wash up in this position. Thus, *Cassiopea* represent a remarkable case of inverted morphology and behaviour among extant scyphozoans. These "upside-down" medusae rest with their subumbrellar surface in contact with the substrate and keep the bell oriented downward, a posture that enhances light exposure for their photosymbiotic algae (Medina et al., 2021; Ohdera et al., 2018). This benthic mode of life, involving continuous interaction between the subumbrellar region and the sediment, produces distinctive taphonomic patterns compared to those of pelagic jellyfish. From a taphonomic perspective, *Cassiopea* provides a valuable modern analogue for understanding how body orientation and life position can influence the final disposition and preservation of medusozoan remains. Fossil jellyfish or discoidal structures preserved in subumbrellar position may reflect ecological and functional adaptations similar to those of *Cassiopea*, where the inverted posture serves as a key adaptive trait. Thus, it is possible that Cambrian jellyfish could have swum in a similar way.

From another perspective, the strong correlation between the length and width of the specimens suggests an isometric growth pattern. This type of growth has been observed in several scyphozoan jellyfish, such as *Stomolophus*, where it has been frequently noted in female specimens, especially when the jellyfish population is in good health (Apolinar Romo, 2021). In the case of *Aurelia aurita*, the proportional growth of its different body parts occurs when the specimens reach adulthood (Kinoshita et al., 1997).

On the other hand, the analysis of the expanded spatial window through spatial modelling has yielded a very compelling result: only about 16 additional jellyfish are expected to be present at the site, with only six specimens located outside the original window. These figures are significant because, as mentioned earlier, we initially identified 14 possible additional specimens beyond those we could definitively confirm. This finding demonstrates how the use of statistical techniques in this type of palaeontological contexts (Boan et al., 2024; Boan et al., 2023; Coutts et al., 2018; Dhungana and Mitchell, 2021; Kolesnikov, 2022; Mitchell et al., 2015; Mitchell and Butterfield, 2018; Mitchell and Kenchington, 2018; Pohle et al., 2020; Rojas et al., 2020) can be highly valuable—not only for analysing spatial point patterns themselves but also for assessing the potential degree of disturbance in these patterns and evaluating the characteristics of undocumented areas.

In this context, the Constantina assemblage exemplifies a high-energy, sandstone-hosted impression paradigm that contrasts markedly with the classic Burgess Shale–type (BST) preservation mode in low-energy, anoxic mudstones (Gaines et al., 2012; Gaines et al., 2008). In the Constantina–Zabriskie–Potsdam model, medusae were stranded in marginal-marine to shoreface settings and rapidly buried by event-driven siliciclastic sedimentation, producing mouldic impressions that faithfully record overall bell morphology, radial structures, and in some cases marginal tentacles, but rarely preserve soft-tissue ultrastructure or carbonaceous films.

Taphonomic fidelity in this paradigm is therefore predominantly morphological and sedimentary, capturing organism–substrate interactions (e.g., deformation of lamination, preferred orientation, clustering) and providing robust palaeoecological signals related to transport dynamics, hydrodynamic reworking, and mass-mortality stranding events. By contrast, BST preservation occurs in distal, low-

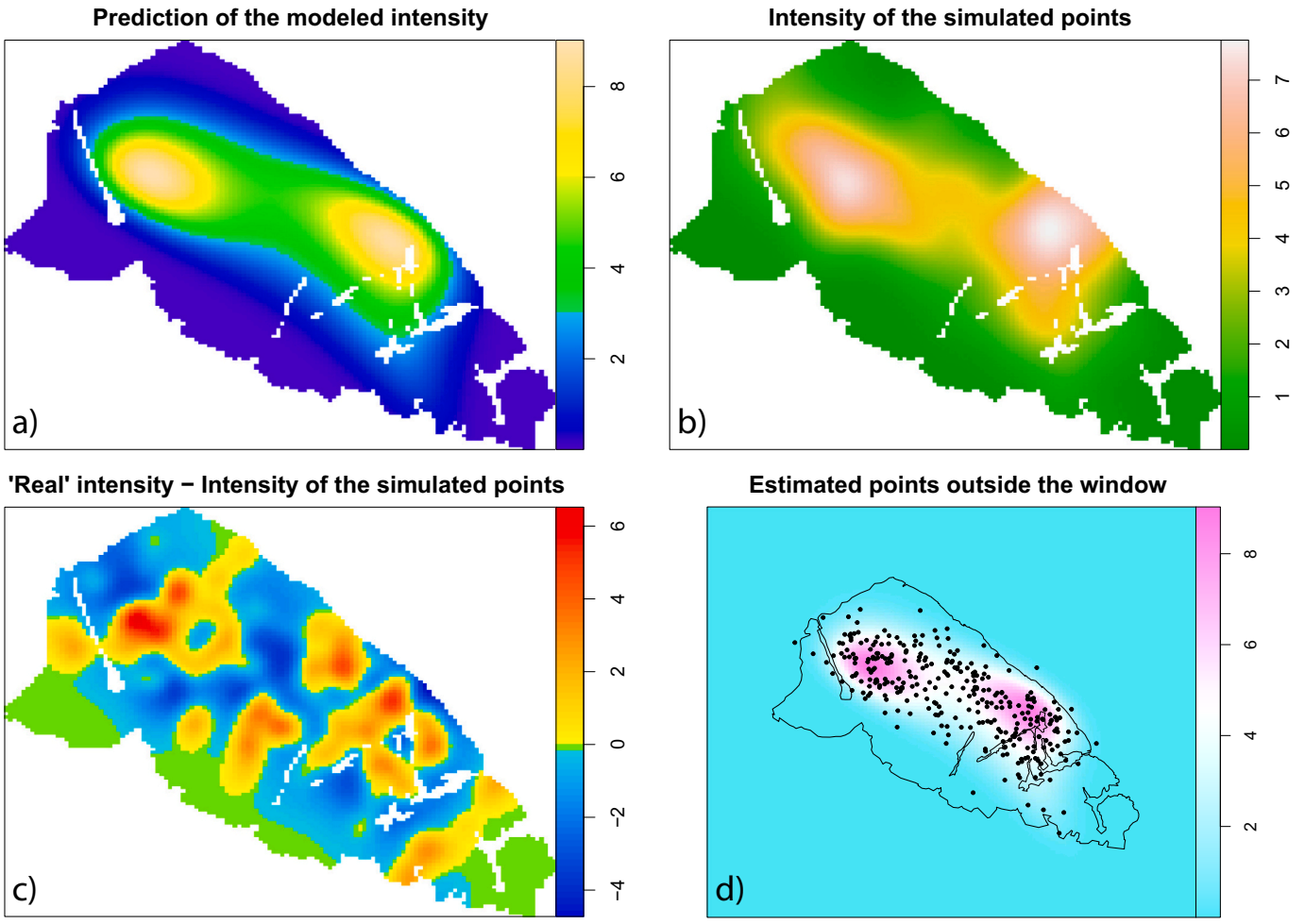

Fig. 14. a) Estimated intensity of the point process based on the fitted model, b) simulation of a new point pattern using the fitted model with the Metropolis-Hastings algorithm, c) a difference map subtracting the intensity of the simulated new point pattern from the "real" intensity of the spatial point pattern and d) an extrapolated estimation of potential points within a larger spatial window (525 m^2) than the original one, which is included in the plot for analytical purposes.

energy basinal settings under dysoxic to anoxic conditions, where rapid burial by fine-grained muds and early diagenetic mineral stabilisation enable the conservation of delicate soft tissues as carbonaceous compressions. This pathway yields exceptional anatomical fidelity, including internal organs and fine tentacular structures, and thus offers unparalleled insight into medusozoan anatomy and phylogenetic affinities (Moon et al., 2023). However, BST assemblages generally provide more limited direct evidence of hydrodynamic transport or shoreline accumulation processes.

Consequently, the high-energy sandstone impression model and the BST carbonaceous compression paradigm represent complementary preservational windows: the former emphasizes spatial patterning, population structure, and event dynamics in marginal-marine contexts, whereas the latter maximizes anatomical detail and evolutionary information within low-energy offshore environments.

6. Conclusions

The comprehensive revaluation of the early Cambrian medusozoan site at Constantina, incorporating advanced statistical and spatial analyses, has not only increased the known specimen count but also revealed new insights into the population structure, morphotype distribution, and taphonomic patterns. The predominance of smaller, exumbrellar morphotypes alongside the occasional larger subumbrellar individuals, combined with isometric growth trends, suggests that these populations were largely composed of healthy, adult individuals, likely females. The clear NW–SE orientation of fossils consistent with palaeocurrent directions points to transport and reorientation mechanisms analogous to those observed in modern jellyfish mass-mortality events. Clustering in discrete areas indicates the role of a common accumulation agent, hinting at behavioural or ecological aggregation prior to burial.

Overall, these findings provide a valuable framework for interpreting medusozoan palaeoecology in early Cambrian ecosystems. Quantitative morphometric and spatial data can inform models of population dynamics, life history strategies, and responses to environmental stress. Furthermore, the integration of modern analogues—such as scyphozoan behaviour under mass-mortality scenarios—allows for more nuanced reconstructions of ancient jellyfish ecology, including aspects of aggregation, transport, and orientation post-mortem. Continued application of such multidisciplinary approaches could illuminate the evolutionary drivers of medusozoan morphology and behaviour, bridging the gap between fossil evidence and extant ecological patterns.

Declaration of generative AI and AI-assisted technologies in the manuscript preparation process

During the preparation of this work the authors used Gemini 3 Flash in order to standardise the text to British English conventions and perform final proofreading to identify typographical errors and misspellings. After using this tool, the authors reviewed and edited the content as needed and take full responsibility for the content of the published article.

CRediT authorship contribution statement

Abel Moclán: Software, Methodology, Investigation, Formal analysis, Data curation, Conceptualization, Writing – original draft. **Alejandro Velázquez-Tello:** Visualization, Software, Methodology, Data curation. **José Ángel Correa-Cano:** Visualization, Software, Methodology, Data curation. **Eduardo Mayoral:** Supervision, Resources, Project administration, Funding acquisition, Conceptualization. **Eduardo MAYORAL:** Writing – original draft. **Alejandro VELÁZQUEZ-TELLO:** Writing – review & editing. **José Ángel CORREA-CANO:** Writing – review & editing.

Declaration of competing interest

The authors declare the following financial interests/personal relationships which may be considered as potential competing interests:

Abel Moclan reports financial support was provided by Fyssen Foundation. Eduardo Mayoral reports administrative support was provided by Territorial Delegation of Sustainability, Environment, and Blue Economy of the Junta de Andalucía. Eduardo Mayoral reports administrative support was provided by Sierra Morena de Sevilla Natural Park. Alejandro Velazquez-Tello reports a relationship with Territorial Delegation of Sustainability, Environment, and Blue Economy of the Junta de Andalucía that includes: employment. Jose Angel Correa reports a relationship with Territorial Delegation of Sustainability, Environment, and Blue Economy of the Junta de Andalucía that includes: employment. If there are other authors, they declare that they have no known competing financial interests or personal relationships that could have appeared to influence the work reported in this paper.

Acknowledgments

This paper was made possible thanks to the support of the Junta de Andalucía for the Research Group RNM 276 and the Scientific and Technological Centre of Huelva (CCTH). We also thank to Inmaculada Gallardo from the Territorial Delegation of Sustainability, Environment, and Blue Economy of the Junta de Andalucía and to Vicente Castaño, Director of the Sierra Morena de Sevilla Natural Park. The authors are very grateful to Cinta Martín from the Intervention Centre of the Andalusian Institute of Historical Heritage for her work during the initial cleaning phases of the site and to the Department of Earth Sciences at the University of Huelva for lending us the total station during the initial spatial documentation phase of this project. The authors would also like to thank the editor, Lucia Angiolini, and the anonymous reviewers for their comments, which have greatly helped to improve the manuscript. In terms of specific funding, AM is funded by a postdoctoral research grant by the Fyssen Foundation.

Appendix A. Supplementary data

Supplementary data to this article can be found online at https://doi.org/10.1016/j.palaeo.2026.113802.

Data availability

The authors confirm that all data necessary for supporting the scientific findings of this paper have been provided.

References

Apolinar Romo, A.A., 2021. Aspectos biológico-pesqueros de la medusa bola de cañon, *Stomolophus* sp. 1, en el Alto Golfo de California (Tesis de maestría). Centro de Investigaciones Biológicas del Noroeste, S.C., México.

Arteaga-Brieba, A., Courtenay, L.A., Cobo-Sánchez, L., Rodríguez-Hidalgo, A., Saladié, P., Ollé, A., Mosquera, M., 2023. An archaeostratigraphic consideration of the Gran Dolina TD10.2 cultural sequence from a quantitative approach. Quat. Sci. Rev. 309, 108033. https://doi.org/10.1016/j.quascirev.2023.108033.

Baddeley, A., Turner, R., 2005. spatstat: an r package for analyzing spatial point patterns. J. Stat. Softw. 12, 1–42. https://doi.org/10.18637/jss.v012.i06.

Baddeley, A., Rubak, E., Turner, R., 2016. Spatial Point Patterns: Methodology and Applications with R. CRC Press, USA.

Betti, F., Bo, M., Enrichetti, F., Manuele, M., Cattaneo-Vietti, R., Bavestrello, G., 2019. Massive strandings of *Velella velella* (hydrozoa: Anthoathecata: Porpitidae) in the Ligurian Sea (North-western Mediterranean Sea). Eur. Zool. J. 86, 343–353. https://doi.org/10.1080/24750263.2019.1671506.

Boan, P.C., Evans, S.D., Hall, C.M.S., Droser, M.L., 2023. Spatial distributions of tribrachidium, rugoconites, and obamus from the Ediacara member (Rawnsley Quartzite), South Australia. Paleobiology 49, 601–620. https://doi.org/10.1017/pab.2023.9.

Boan, P.C., Evans, S.D., Droser, M.L., 2024. And now for something completely random: Spatial distribution of Dickinsonia on the Ediacaran seafloor. Glob. Planet. Chang. 238, 104467. https://doi.org/10.1016/j.gloplacha.2024.104467.

Buatois, L.A., Gingras, M.K., Maceachern, J., Mángano, M.G., Zonneveld, J.-P., Pemberton, S.G., Netto, R.G., Martin, A., 2005. Colonization of Brackish-Water systems through time: evidence from the Trace-Fossil record. PALAIOS 20, 321–347. https://doi.org/10.2110/palo.2004.p04-32.

Cartwright, P., Halgedahl, S.L., Hendricks, J.R., Jarrard, R.D., Marques, A.C., Collins, A. G., Lieberman, B.S., 2007. Exceptionally preserved jellyfishes from the middle Cambrian. PLoS One 2, e1121. https://doi.org/10.1371/journal.pone.0001121.

Cobo-Sánchez, L., Aramendi, J., Domínguez-Rodrigo, M., 2014. Orientation patterns of wildebeest bones on the lake Masek floodplain (Serengeti, Tanzania) and their relevance to interpret anisotropy in the Olduvai lacustrine floodplain. Quat. Int. 322–323, 277–284. https://doi.org/10.1016/j.quaint.2013.07.130.

Cobo-Sánchez, L., Domínguez-Rodrigo, M., Mabulla, A., Baquedano, E., 2024. Chapter 5 - Reconstructing early human behavior through the in-site spatial statistical analysis of DS. In: Domínguez-Rodrigo, M., Cobo-Sánchez, L., Baquedano, E., Mabulla, A., Gidna, A., Diez-Martín, F. (Eds.), Reconstructing Olduvai. Academic Press, pp. 197–240. https://doi.org/10.1016/B978-0-443-27382-7.00007-1.

Coutts, F.J., Bradshaw, C.J.A., García-Bellido, D.C., Gehling, J.G., 2018. Evidence of sensory-driven behavior in the Ediacaran organism Parvancorina: Implications and autecological interpretations. Gondwana Res. 55, 21–29. https://doi.org/10.1016/j.gr.2017.10.009.

Crimes, T.P., Herdman, J., 1970. Trilobite tracks and other trace fossils from the upper Cambrian of North Wales. Geol. J. 7, 47–68. https://doi.org/10.1002/gj.3350070104.

Devereux, M.G., 2001. Palaeoecology of the Middle Cambrian Raymond Quarry Fauna, Burgess Shale, British Columbia (M. Sc. dissertation). University of Western Ontario, Ontario.

Dhungana, A., Mitchell, E.G., 2021. Facilitating corals in an early Silurian deep-water assemblage. Palaeontology 64, 359–370. https://doi.org/10.1111/pala.12527.

Diez-Martín, F., Cobo-Sánchez, L., Baddeley, A., Uribelarrea, D., Mabulla, A., Baquedano, E., Domínguez-Rodrigo, M., 2021. Tracing the spatial imprint of Oldowan technological behaviors: a view from DS (Bed I, Olduvai Gorge, Tanzania). PLoS One 16, e0254603. https://doi.org/10.1371/journal.pone.0254603.

Domínguez-Rodrigo, M., García-Pérez, A., 2013. Testing the accuracy of different A-Axis types for measuring the orientation of bones in the archaeological and paleontological record. PLoS One 8, e68955. https://doi.org/10.1371/journal.pone.0068955.

Domínguez-Rodrigo, M., Uribelarrea, D., Santonja, M., Bunn, H.T., García-Pérez, A., Pérez-González, A., Panera, J., Rubio-Jara, S., Mabulla, A.Z.P., Baquedano, E., Yravedra, J., Díez-Martín, F., 2014. Autochthonous anisotropy of archaeological materials by the action of water: experimental and archaeological reassessment of the orientation patterns at the Olduvai sites. J. Archaeol. Sci. 41, 44–68. https://doi.org/10.1016/j.jas.2013.07.025.

Domínguez-Rodrigo, M., Cobo-Sánchez, L., Yravedra, J., Uribelarrea, D., Arriaza, M.C., Organista, E., Baquedano, E., 2018. Fluvial spatial taphonomy: a new method for the study of post-depositional processes. Archaeol. Anthropol. Sci. 10, 1769–1789. https://doi.org/10.1007/s12520-017-0497-2.

Fedonkin, M.A., 1985. Sistematičeskoe opisanie vendskih Metazoa. In: Sokolov, B.S., Ivanovskiy, A.B. (Eds.), Vendskaâ Sistema. Paleontologičeskoe i Istoriko-Geologičeskoe Obosnovanie. T. I. Nauka, Moscow, pp. 70–106.

Fernández-López, S.R., Fernández-Jalvo, Y., Alcalá, L., 2002. Accumulation: taphonomic concept and other palaeontological uses. In: De Renzi, M., Pardo Alonso, M.V., Belinchón, M., Peñalver, E., Montoya, P., Márquez-Aliaga, A. (Eds.), Current Topics on Taphonomy and Fossilization. Presented at the I Congreso Internacional de Tafonomía, Ayuntamiento de Valencia, Valencia, pp. 37–47.

Fossette, S., Gleiss, A.C., Chalumeau, J., Bastian, T., Armstrong, C.D., Vandenabeele, S., Karpytchev, M., Hays, G.C., 2015. Current-Oriented swimming by jellyfish and its role in bloom maintenance. Curr. Biol. 25, 342–347. https://doi.org/10.1016/j.cub.2014.11.050.

Fu, D., Tong, G., Dai, T., Liu, W., Yang, Y., Zhang, Y., Cui, L., Li, L., Yun, H., Wu, Y., Sun, A., Liu, C., Pei, W., Gaines, R.R., Zhang, X., 2019. The Qingjiang biota—a burgess shale–type fossil Lagerstätte from the early Cambrian of South China. Science 363, 1338–1342. https://doi.org/10.1126/science.aau8800.

Gaines, R.R., Briggs, D.E.G., Yuanlong, Z., 2008. Cambrian burgess shale-type deposits share a common mode of fossilization. Geology 36, 755–758. https://doi.org/10.1130/G24961A.1.

Gaines, R.R., Hammarlund, E.U., Hou, X., Qi, C., Gabbott, S.E., Zhao, Y., Peng, J., Canfield, D.E., 2012. Mechanism for burgess shale-type preservation. Proc. Natl. Acad. Sci. 109, 5180–5184. https://doi.org/10.1073/pnas.1111784109.

Gámez Vintaned, J.A., Liñán, E., 1996. Significant ichnological data during the Neoproterozoic-early Cambrian transition in Iberia. In: Liñán, E., Gámez Vintaned, J. A., Gozalo, R. (Eds.), II Field Conference of the Cambrian Stage Subdivision Working

Groups. International Subcommission on Cambrian Stratigraphy. Spain, 13-21 September 1996. Universidad de Zaragoza, Zaragoza, pp. 101–102. Field Trip Guide and Abstracts.
Gemmell, B.J., Costello, J.H., Colin, S.P., Stewart, C.J., Dabiri, J.O., Tafti, D., Priya, S., 2013. Passive energy recapture in jellyfish contributes to propulsive advantage over other metazoans. Proc. Natl. Acad. Sci. 110, 17904–17909. https://doi.org/10.1073/pnas.1306983110.
Hagadorn, J.W., Belt, E.S., 2008. Stranded in upstate New York: Cambrian scyphomedusae from the Potsdam sandstone. PALAIOS 23, 424–441. https://doi.org/10.2110/palo.2006.p06-104r.
Hagadorn, J.W., Dott Jr., R.H., Damrow, D., 2002. Stranded on a late cambrian shoreline: Medusae from Central Wisconsin. Geology 30, 147–150. https://doi.org/10.1130/0091-7613(2002)030%253C0147:SOALCS%253E2.0.CO;2.
Hammer, Ø., Harper, D.A.T., Ryan, P.D., 2001. PAST: PAleontological STastistics Software package for education and data analysis. Palaeontol. Electron. 4, 9. http://palaeo-electronica.org/2001_1/past/issue1_01.htm.
Han, J., Hu, S., Cartwright, P., Zhao, F., Ou, Q., Kubota, S., Wang, X., Yang, X., 2016. The earliest pelagic jellyfish with rhopalia from Cambrian Chengjiang Lagerstätte. Palaeogeogr. Palaeoclimatol. Palaeoecol. 449, 166–173. https://doi.org/10.1016/j.palaeo.2016.02.025.
Jones, T., Parrish, J.K., Burgess, H.K., 2021. Long-term patterns of mass stranding of the colonial cnidarian *Velella velella*: influence of environmental forcing. Mar. Ecol. Prog. Ser. 662, 69–83. https://doi.org/10.3354/meps13644.
Kinoshita, J., Hiromi, J., Kadota, S., 1997. Do respiratory metabolic rates of the scyphomedusa Aurelia aurita scale isometrically throughout ontogeny in a sexual generation? Hydrobiologia 347, 51–55. https://doi.org/10.1023/A:1002942806113.
Kolesnikov, A., 2022. Beltanelliformis konovalovi sp. nov. from the terminal neoproterozoic of central urals: taphonomic and ecological implications. Front. Earth Sci. 10. https://doi.org/10.3389/feart.2022.875001.
Lacelle, M.A., Hagadorn, J.W., Groulx, P., 2008. The widespread distribution of Cambrian Medusae: scyphomedusa strandings in the Potsdam Group of southwestern Quebec. In: Geological Society of America Abstracts with Programs, p. 371.
Liñán, E., 1978. Bioestratigrafía de la Sierra de Córdoba (Ph.D. dissertation). Universidad de Granada, Granada.
Liñán, E., 1984. Los icnofósiles de la Formación Torreárboles (¿Precámbrico?-Cámbrico inferior) en los alrededores de Fuente de Cantos, Badajoz. cad. Lab. Xeol. Laxe Rev. Xeoloxía Galega E Hercínico Penins. 8, 47–74.
Liñán, E., Gámez Vintaned, J.A., 1993. Lower Cambrian palaeogeography of the Iberian Peninsula and its relations with some neighbouring European areas. Bull. Société Géologique Fr. 164, 831–842.
Liñán, E., Palacios, T., 1983. Aportaciones micropaleontológicas para el conocimientos del límite Precámbrico-Cámbrico en la Sierra de Córdoba. Comun. Serviços Geológicos Port. 69, 227–234.
Luzón, C., Yravedra, J., Courtenay, L.A., Saarinen, J., Blain, H.-A., De Miguel, D., Viranta, S., Azanza, B., Rodríguez-Alba, J.J., Herranz-Rodrigo, D., Serrano-Ramos, A., Solano, J.A., Oms, O., Agustí, J., Fortelius, M., Jiménez-Arenas, J.M., 2021. Taphonomic and spatial analyses from the Early Pleistocene site of Venta Micena 4 (Orce, Guadix-Baza Basin, southern Spain). Sci. Rep. 11, 13977. https://doi.org/10.1038/s41598-021-93261-1.
Martín-Perea, D.M., Courtenay, L.A., Domingo, M.S., Morales, J., 2020. Application of artificially intelligent systems for the identification of discrete fossiliferous levels. PeerJ 8, e8767. https://doi.org/10.7717/peerj.8767.
Mayoral, E., Liñán, E., Gámez Vintaned, J.A., Muñiz, F., Gozalo, R., 2004. Stranded jellyfish in the lowermost Cambrian (Corduban) of Spain. Span. J. Palaeontol. 19, 191–198. https://doi.org/10.7203/sjp.19.2.20531.
Mayoral, E., Liñán, E., Gámez Vintaned, J.A., Gozalo, R., 2008. Medusas del Cámbrico inferior de Constantina (Sevilla). In: Menor, A., Cuenca Bonilla, I., Álvarez, J.A. (Eds.), Investigación científica y conservación en el Parque Natural Sierra Norte de Sevilla. Consejería de Medio Ambiente de la Junta de Andalucía, Sevilla, pp. 45–57.
Mayoral, E., Liñan, E., Santos, A., 2019. The negligence and lazy of the administration: the greatest danger to the conservation of the unique lagerstätte sites. Span. J. Palaeontol. 34, 85–94. https://doi.org/10.7203/sjp.34.1.15243.
Mayoral, E., Liñán, E., Gámez Vintaned, J.A., Gozalo, R., Diez Álvarez, M.E., Santos, A., Collantes, L., Gil Toja, A., 2021. The exceptional fossil record of the sierra norte de sevilla UNESCO global geopark. The early Cambrian of the Constantina-San Nicolás del Puerto Area (Seville Province, Spain). Geoconservation Res. 4, 61–65. https://doi.org/10.30486/gcr.2021.1912341.1046.
Mayoral, E., Liñán, E., Gámez Vintaned, J.A., Gozalo, R., Collantes, L., Velázquez-Tello, A., Correa, J.Á., Moclán, A., Gallardo, I.C., Castaño, V., Bernáldez, E., Moncunill-Solé, B., Blanco, Grandal d'Anglade, A., González Fortes, G., Santos Fidalgo, L., Bao, R., 2024. El monumento natural *Huellas fósiles de medusas de Constantina* (Sevilla). Una referencia en el registro paleontológico mundial. In: Libro de Resúmenes. XXXIX Jornadas de La Sociedad Española de Paleontología, p. 188. Presented at the XXXIX Jornadas de la Sociedad Española de Paleontología, Paleontological Publications, A Coruña.
Medina, M., Sharp, V., Ohdera, A., Bellantuono, A., Dalrymple, J., Gamero-Mora, E., Steinworth, B., Hofmann, D.K., Martindale, M.Q., Morandini, A.C., 2021. The Upside-Down Jellyfish *Cassiopea xamachana* as an Emerging Model System to Study Cnidarian–Algal Symbiosis. In: Handbook of Marine Model Organisms in Experimental Biology. CRC Press, pp. 149–171.
Méndez-Quintas, E., Panera, J., Altamura, F., Di Bianco, L., Melis, R.T., Piarulli, F., Ruta, G., Mussi, M., 2019. Gombore II (Melka Kunture, Ethiopia): a new approach to formation processes and spatial patterns of an Early Pleistocene Acheulean site. J. Archaeol. Sci. 108, 104975. https://doi.org/10.1016/j.jas.2019.104975.
Mielgo, C., Huguet, R., Laplana, C., Martín-Perea, D.M., Moclán, A., Márquez, B., Arsuaga, J.L., Pérez-González, A., Baquedano, E., 2024. Intra-site spatial approaches based on taphonomic analyses to characterize assemblage formation at pleistocene sites: a case study from Buena Pinta Cave (Pinilla del Valle, Madrid, Spain). Archaeol. Anthropol. Sci. 16, 1–28. https://doi.org/10.1007/s12520-023-01913-2.
Mitchell, E.G., Butterfield, N.J., 2018. Spatial analyses of Ediacaran communities at mistaken point. Paleobiology 44, 40–57. https://doi.org/10.1017/pab.2017.35.
Mitchell, E.G., Kenchington, C.G., 2018. The utility of height for the Ediacaran organisms of mistaken point. Nat. Ecol. Evol. 2, 1218–1222. https://doi.org/10.1038/s41559-018-0591-6.
Mitchell, E.G., Kenchington, C.G., Liu, A.G., Matthews, J.J., Butterfield, N.J., 2015. Reconstructing the reproductive mode of an Ediacaran macro-organism. Nature 524, 343–346. https://doi.org/10.1038/nature14646.
Moclán, A., Cobo-Sánchez, L., Domínguez-Rodrigo, M., Méndez-Quintas, E., Rubio-Jara, S., Panera, J., Pérez-González, A., Santonja, M., 2023a. Spatial analysis of an early middle palaeolithic kill/butchering site: the case of the Cuesta de la Bajada (Teruel, Spain). Archaeol. Anthropol. Sci. 15, 91. https://doi.org/10.1007/s12520-023-01792-7.
Moclán, A., Huguet, R., Márquez, B., Álvarez-Fernández, A., Laplana, C., Arsuaga, J.L., Pérez-González, A., Baquedano, E., 2023b. Identifying activity areas in a neanderthal hunting camp (the Navalmaíllo rock shelter, Spain) via spatial analysis. Archaeol. Anthropol. Sci. 15, 44. https://doi.org/10.1007/s12520-023-01746-z.
Moon, J., Caron, J.-B., Moysiuk, J., 2023. A macroscopic free-swimming medusa from the middle Cambrian burgess shale. Proc. R. Soc. B Biol. Sci. 290, 20222490. https://doi.org/10.1098/rspb.2022.2490.
Ohdera, A.H., Abrams, M.J., Ames, C.L., Baker, D.M., Suescún-Bolívar, L.P., Collins, A.G., Freeman, C.J., Gamero-Mora, E., Goulet, T.L., Hofmann, D.K., Jaimes-Becerra, A., Long, P.F., Marques, A.C., Miller, L.A., Mydlarz, L.D., Morandini, A.C., Newkirk, C. R., Putri, S.P., Samson, J.E., Stampar, S.N., Steinworth, B., Templeman, M., Thomé, P.E., Vlok, M., Woodley, C.M., Wong, J.C.Y., Martindale, M.Q., Fitt, W.K., Medina, M., 2018. Upside-down but headed in the right direction: review of the highly versatile Cassiopea xamachana system. Front. Ecol. Evol. 6. https://doi.org/10.3389/fevo.2018.00035.
Perejón, A., 1984. Bioestratigrafía de los arqueociatos en España. Cuad. Geol. Ibérica 9, 213–266.
Pohle, A., Fuchs, D., Korn, D., Klug, C., 2020. Spatial distribution of oncocerid cephalopods on a middle Devonian bedding plane suggests semelparous life cycle. Sci. Rep. 10, 2847. https://doi.org/10.1038/s41598-020-59507-0.
R Core Team, 2022. R: A Language and Environment for Statistical Computing.
Richter, R., 1937. Marken und spuren aus allen zeiten. I-II. Senckenbergiana 19, 150–169.
Richter, R., Richter, E., 1940. Die Saukianda-Stufe von Andalusien, eine fremde Fauna im europäischen Ober-Kambrium, Abh. Senckenb. Naturforsch. Ges. Senckenbergische Naturforschende Ges.
Ritter, J.R., 1972. Cyclic sedimentation in Agua Hedionda lagoon, southern California. J. Waterw. Harb. Coast. Eng. Div. 98, 597–602. https://doi.org/10.1061/AWHCAR.0000170.
Rojas, A., Dietl, G.P., Kowalewski, M., Portell, R.W., Hendy, A., Blackburn, J.K., 2020. Spatial point pattern analysis of traces (SPPAT): an approach for visualizing and quantifying site-selectivity patterns of drilling predators. Paleobiology 46, 259–271. https://doi.org/10.1017/pab.2020.15.
Sánchez-Romero, L., Benito-Calvo, A., Marín-Arroyo, A.B., Agudo-Pérez, L., Karampaglidis, T., Rios-Garaizar, J., 2020. New insights for understanding spatial patterning and formation processes of the Neanderthal occupation in the Amalda I cave (Gipuzkoa, Spain). Sci. Rep. 10, 8733. https://doi.org/10.1038/s41598-020-65364-8.
Sappenfield, A.D., Tarhan, L.G., Droser, M.L., 2017. Earths oldest jellyfish strandings: a unique taphonomic window or just another day at the beach? Geol. Mag. 154, 859–874. https://doi.org/10.1017/S0016756816000443.
Sdzuy, K., 1962. Trilobiten aus dem Unter-Kambrium der Sierra Morena (S-Spanien). Senckenb. Lethaea 43, 181–229.
Tarhan, L.G., Hagadorn, J.W., 2008. Taphonomy and classification of medusae from the Late Cambrian of Wisconsin and New York. In: Geological Society of America Abstracts with Programs, p. 80.
van den Berg, J.H., Nio, S.D., 2010. Sedimentary Structures and Their Relation to Bedforms and Flow Conditions. EAGE. https://doi.org/10.3997/9789462820180.
Vyalov, O.S., 1971. Redkie problematiki iz mezozoja Pamira i Kavkaza. Paleontol. Sb. Izd. L'vovskogo Univ. 7, 85–93.
Wickham, H., 2016. ggplot2: Elegant Graphics for Data Analysis, Use R. Springer, New York. https://doi.org/10.1007/978-0-387-98141-3_1.
Wiegand, T., Moloney, K.A., 2013. Handbook of spatial Point-Pattern analysis in ecology. Chapman and Hall/CRC, New York. https://doi.org/10.1201/b16195.
Young, G.A., Hagadorn, J.W., 2010. The fossil record of cnidarian medusae. Palaeoworld, "fossil corals, archaeocyaths and sponges". In: Proceedings of the 10th International Symposium on Fossil Cnidaria and Porifera 19, pp. 212–221. https://doi.org/10.1016/j.palwor.2010.09.014.